DNA Strand Breaks and Gaps Direct Retroviral Integration

Gayan Senavirathne[1], Anne Gardner[1], James London[1], Richard Fishel[1,*] and Kristine E. Yoder[1,*]

[1]Molecular Carcinogenesis and Chemoprevention Program, The James Comprehensive Cancer Center and Ohio State University, Columbus, OH 43210, US

*Correspondence may also be addressed to: R. Fishel (rafishel@gmail.com) or K.E. Yoder (yoder.176@osu.edu)

Integration into the host genome is essential for retrovirus infection and is catalyzed by a nucleoprotein complex (Intasome) containing the virus-encoded integrase (IN) and the reverse transcribed (RT) viral copy DNA (cDNA). Previous studies suggested that intasome integration was limited DNA site recognition. Using high resolution single molecule Förster resonance energy transfer (smFRET), we show that Prototype Foamy Virus (PFV) intasomes pause at sites containing DNA strand breaks and gaps. These strand discontinuities are similar to intermediates produced by base excision repair (BER) lesion processing, which has been shown to affect retrovirus integration *in vivo*. Intasome pausing targeted site-directed integration without inducing significant cDNA-intasome conformational alterations. The 8-oxo-guanine BER-recognized lesion, a mismatch, or a +T nucleotide insertion that induce backbone flexibility and/or static bends did not enhance intasome pausing. However, a 5'-phosphate within the break/gap diminished site-directed integration. These results suggest that dynamic intasome-DNA interactions may be modulated to target retroviral integration. (152 words)

Retroviruses must integrate into a host genome to cause clinically significant diseases such as AIDS or leukemia [1]. Retroviral integration is catalyzed by a poorly understood pre-integration complex (PICs) that at a minimum consists of viral integrase (IN) multimers in complex with the two long terminal repeat (LTR) sequences that flank the viral cDNA, termed an intasome [2-4]. The IN protein initially excises two nucleotides (nt) from the LTR [5] producing recessed 3'-OH's that provide the substrate for integration. Consecutive IN-catalyzed S_N2 strand transfer reactions then covalently link the recessed 3'-LTR ends across one major groove of a target DNA separated by 4-6 bp, depending on the retrovirus genera [4,6,7]. When unraveled the newly integrated provirus is flanked by 4-6 nt gaps containing 2 nt 5'-flaps that are restored to fully duplex DNA by the host DNA repair machinery [8-10].

Alignment of many integration sites suggests that most retroviruses prefer to integrate at degenerate DNA sequences that for HIV-1 often positions a guanine (G) adjacent to the strand transfer site (T c **G** * G/t T N A C * C/a g A; uppercase favored, lowercase disfavored, * strand transfer site) [11,12]. A large-scale siRNA screen identified base excision repair (BER) components as the most frequent DNA repair genes that altered HIV integration efficiency [8]. Of these, mutation of BER glycosylases *OGG1* or *MUTYH* reduced HIV-1 integration and eliminated the preference for G adjacent to the strand transfer site [9]. The OGG1 glycosylase principally excises 8-oxo-guanine (8-oxo-G) residues in DNA that are the most frequent oxidative damage in cells [13,14]. The MUTYH glycosylase excises adenine (A) residues that are frequently misincorporated across from an 8-oxo-G lesion during replication. Mutation of the BER polymerase β (*Polβ*) also significantly decreased HIV-1 integration [15]. However, the phenotype was linked to the 5'-deoxyribose phosphate (5'-dRP) lyase activity and not the polymerase activity of Polβ [15]. The 5'-dRP lyase removes the deoxyribose sugar and associated phosphate leaving a 1 nt gap in the DNA after base excision by a glycosylase, [16-18]. Interestingly, OGG1 also contains an intrinsic 5'-dRP lyase that could be employed during MUTYH collaborative oxidative damage processing [15].

Historical studies have suggested that bent or flexible DNA is a favored target for retroviral integration *in vivo* [19,20] and *in vitro* [21-28]. Prototype foamy virus (PFV) is a member of the *spumavirus* genera and has been extensively studied since it shares similar catalytic site geometry, chemistry and therapeutic inhibitor sensitivity with the pathogenic lentivirus HIV-1 [29-31]. Structures of the PFV intasome target capture complex (TCC) and the strand transfer complex (STC) have been solved and represent key steps that provide a biophysical window into retroviral integration [21,29]. While several single molecule studies have detailed the dynamic progressions between PFV intasome and target DNA [22,28], the DNA configurations that drive rate-limiting integration site choice remain enigmatic.

RESULTS

PFV intasomes transiently pause at nicks and gaps in the DNA. A single molecule Förster resonance energy transfer (smFRET) system [32] was developed to probe the real-time interactions between a purified PFV intasome with DNA containing a variety of DNA lesions and BER intermediates that introduce localized bends or flexibility into DNA [33-36] (**Fig. 1a**; **Extended Data Table 1**). PFV intasomes were assembled with pre-processed recessed 3'-OH viral 5'-LTR oligonucleotides (vDNA) containing a Cy3 FRET-donor flourophore on the non-transferred strand 11 bp from the 3'-end (Cy3-PFV). We confirmed that concerted integration of the Cy3-PFV intasomes into a supercoiled target DNA mimicked unlabeled PFV intasomes, suggesting that the Cy3-labeled vDNA does not affect integration activity (**Extended Data Fig. 1**) [22].

A 60 bp target DNA containing defined lesions was synthesized that contained a Cy5 FRET-acceptor flourophore located on the undamaged strand 11 bp 5' of the lesion as well as an Alexa488 marker flourophore on the damaged strand 3 bp from the 3' end (**Fig. 1a**, **Extended Data Table 1**). This target DNA was bound to a passivated smFRET flow cell surface at the 5'-end of the lesion-containing strand and purified Cy3-PFV intasomes infused and illuminated with a 532 nm laser. Binding of the Cy3-PFV intasomes near the lesion results in Cy5 (660 nm) FRET emission events consistent with dynamic TCC interactions (**Fig. 1b and 1c**, left; 100 msec frame rate). Background correction and Hidden Markov Modeling (HMM) generated a transition density plot [37] that was used to determine FRET efficiency (*E*) and reversibility (**Fig. 1c**, middle; **Extended Data Fig. 2 and 3**). The total number of FRET events (n) from numerous DNA molecules (N) were aligned to the PFV intasome infusion time to produce a post-synchronized histogram (N = 552, n = 46; **Fig. 1c**, right) [38]. A narrow range of Cy5 fluorescence ($E \sim 0.06$) was detected in both the transition density plot and post-synchronized histogram that after inspection of the real-time movies were found to represent excursions of free Cy3-PFV intasome aggregates across the evanescent field containing the target DNA (**Extended Data Movie 1**). These events were easily recognized since they saturated the Cy3 channel and bled into the Cy5 channel producing

a pseudo-FRET signal (**Fig. 1c**, right). Rare higher FRET events (E > 0.1) were detected that appeared to correspond to PFV intasome binding and dissociation events near the Cy5 fluorophore on the DNA (**Fig. 1c**, right). A similar pattern was observed when an 8-oxo-G/C, a G/T mismatch or +T nucleotide insertion was present in the duplex target DNA (**Extended Data 4a-c**). The lack of significant FRET events above the pseudo-FRET background suggests very little if any specific PFV intasome binding to these target DNA substrates.

In contrast, a DNA substrate containing a 1 nt gap with a 3'-hydoxyl and 5'-phosphate [1 nt GAP (5'-P)] similar to a 5'-dRP lyase BER intermediate consistently displayed bursts of Cy3-PFV binding events accompanied by Cy5 FRET events (**Fig. 1d,** left). Inspection of real-time movies confirmed that these FRET events represented PFV intasome-lesion interactions arising from colocalized diffraction-limited Cy3-Cy5 spots (**Extended Data Movie 2**). The FRET bursts from individual traces (**Fig. 1d**, center) converged into a distinct ensemble FRET peak that was clearly separate from the pseudo-FRET background ($E_{1nt\ Gap\ (5'\text{-}P)}$ ~ 0.16 ± 0.05; N = 540, n = 3267; **Fig. 1d**, right; **Extended Data Table 4**). These events are consistent with the formation of a stably but transient TCC, with the PFV intasome bound near the DNA lesion (**Fig. 1b**; **Fig. 1d**). DNA substrates containing a single-strand scission [Nick (5'-P); $E_{Nick\ (5'\text{-}P)}$ ~ 0.15 ± 0.08; N = 549, n = 1084], a 2 nt gap [2 nt GAP (5'-P); $E_{2nt\ Gap(5'\text{-}P)}$ ~ 0.18 ± 0.10; N = 474, n = 1175] as well as a 5'-phosphate free nick ($E_{Nick\ (5'\text{-}OH)}$ ~ 0.17 ± 0.07; N = 558, n = 507), 1 nt gap ($E_{1nt\ Gap\ (5'\text{-}OH)}$ ~ 0.19 ± 0.05; N = 496, n = 2784) and 2 nt gap ($E_{2nt\ Gap\ (5'\text{-}OH)}$ ~ 0.23 ± 0.11; N = 540, n = 799) also yielded significant FRET events consistent with the formation of a TCC (**Extended Data Fig. 4d-h**; **Extended Data Table 2**). Importantly, the number of FRET transitions per molecule also increased with DNA substrates that displayed clear binding events (**Extended Data Fig. 5**). The consistent peak of FRET efficiency suggests the Cy3-PFV intasomes bind within a narrow distance around the DNA lesions.

To quantify the relative binding efficiency of PFV intasomes to the DNA lesions, we normalized the frequency of TCC FRET binding events to the pseudo-FRET excursion events

that appear relatively constant between target DNA substrates at a fixed Cy3-PFV intasome concentration and frame rate (**Fig. 1e-g**; **Extended Table 3**). As expected, there were few FRET events outside the normalized pseudo-FRET peak when duplex DNA, DNA containing an 8-oxo-G/C lesion, a G/T mismatch or a +T nucleotide insertion were examined (E > 0.1; **Fig. 1e**; **Extended Data Fig. 6a-d**). Since the G/T mismatch introduces significant local flexibility into the DNA [39,40] and the +T insertion produces a relatively stable 22° DNA bend [41], these observations suggest that the preference for flexible or bent DNA by retrovirus intasomes [19,42,43] may be more subtle than previously appreciated.

In contrast, a nick, 1 nt gap or 2 nt gap, with or without the 5'-P, displayed normalized FRET peaks that were clearly separated from the pseudo-FRET background (**Fig. 1f,g**; **Extended Data Fig. 6e-j**). The relative frequency of these TCC events suggested that Cy3-PFV preferred a 1 nt Gap >> nick ≥ 2 nt Gap. We noted a broadening of the normalized TCC FRET peak as well as an increased average FRET efficiency with target DNA containing a 2 nt GAP (**Fig. 1f,g**). Because the 2 nt Gap extends further toward the Cy5 FRET acceptor, these results suggest an increase in the number of different asymmetric binding events that on average bind closer to the Cy5 fluorophore and 5' of the gap. The post-synchronized histograms and the relative binding efficiency pattern of TCC FRET events was similar at a 1 sec frame rate (**Extended Data Fig. 7**; **Extended Table 4**). Because of the potential for enhanced resolution we chose a 100 msec frame rate for the majority of these studies.

Using HMM we determine the binding (τ_{on}) and dissociation (τ_{off}) kinetics (**Extended Data Fig. 8a**). As expected, the binding events to an 8-oxo-G/C, a G/T mismatch or a +T nucleotide insertion were extremely rare, often < 1 event per molecule over the 3 min observation window, making any τ_{on} and τ_{off} values statistically insignificant (**Extended Data Fig. 5a-d**; **Extended Data Fig. 8b**). However, the 1 nt GAP (5'-P) and 1 nt Gap (5'-OH) experienced an average of ~6 binding events per molecule with a distribution of 1-14 binding events for the vast majority of

molecules (**Extended Data Fig. 5f,i**). Less, but statistically significant binding events were recorded for DNAs containing a nick and 2 nt gap regardless of the presence of a 5'-phosphate within the lesion (**Extended Data Fig. 6e,g,i,j**). Fitting these events to a single exponential decay resulted in a τ_{on} that varied from 0.3 - 0.75 sec and an τ_{off} that varied from 7 - 24 sec (**Fig. 1h,i**; **Extended Data Fig. 8c-h**). We note that the τ_{on} events for the 2 nt gap substrates approached the frame rate which appears to reduce the number of recorded events, and in the case of the 2 nt GAP (3'-OH) artificially increased the τ_{off} (**Fig. 1h,i**; **Extended Data Fig. 8e,h**). Blocking the open end of the 1nt GAP (5'-OH) DNA substrate to trap intasomes diffusing along the DNA [44] did not significantly alter the distribution of events per molecule or the post-synchronized FRET histogram (**Extended Data Fig. 9a,b**). However, while the τ_{on} remained largely constant the τ_{off} significantly decreased (**Fig. 1h.i**; **Extended Data Fig. 9c-e**), resulting in an increased number of normalized lesion binding events (**Fig. 1j**). These observations suggest that at least a fraction of the Cy3-PFV intasomes that form a TCC may dissociate by sliding off the ends of the lesion containing oligonucleotide.

Integration of PFV intasomes occurs at the pause site. Integration by the Cy3-PFV intasomes forms a strand transfer complex (STC) that results in prolonged FRET events (**Fig. 2a,b**). These sustained FRET events often ended with photobleaching of the Cy3 or Cy5 fluorophores on the intasome or the target DNA substrate (**Fig. 2c**). Post-synchronized histograms displayed well defined STC FRET events for several of the DNA substrates, where both the frequency and FRET efficiency could be quantified (**Fig. 2d,e**; **Extended Data Table 2**). We found that the FRET efficiency of TCC events (E_{TCC}) was nearly identical to the STC events (E_{STC}; **Extended Data Table 2**). Where it differed, for example the Nick (5'-P) DNA substrate, the number of events were extremely low ($n < 5$) making interpretation of the histograms impractical (**Extended Data**

Fig. 10). The consistency in FRET efficiencies is consistent with the conclusion that the TCC pausing events contribute to the formation of an STC product.

To confirm that the STC events formed a covalent integration structure we assembled PFV intasomes with viral donor oligonucleotides containing a terminal di-deoxy-adenosine (ddA) (**Fig. 2f,g**; **Extended Data Table 5**). We used the1 nt Gap (5'-OH) target DNA as a model since it displayed the most frequent TCC and STC events. As expected, we observed significant numbers of TCC events that displayed a similar FRET efficiency to *wild type* PFV intasome interactions (compare **Fig. 2f** to **Extended Data Fig. 4g**; **Extended Data Table 2**). However, only two possible STC events were recorded on N = 564 DNA molecules ($STC_{1nt\ Gap\ (5'\text{-}OH)\text{-}ddA}$ = 0.35 ± 0.2%) compared to 20% with *wild type* Cy3-PFV (**Fig. 2g**; **Extended Data Table 5**). This >50-fold reduction in STC events with Cy3-PFV-ddA intasomes strongly suggests that the prolonged FRET events represent covalent STC formation.

To determine whether the positioning of the fluorophore on the target DNA influenced PFV intasome interactions, we moved the Cy5 to 11 bp 3' of the 1 nt Gap (5'-OH) (**Fig. 2h**; **Extended Data Table 1**). Similar TCC FRET events (**Fig. 2i,j**) and STC FRET events (**Fig. 2k,l**) were observed compared to the target DNA containing Cy5 located 11 bp 5' of the 1 nt Gap (5'-OH) (**Extended Fig. 4g**; **Fig. 2e**). Intriguingly, the FRET efficiency of the TCC and STC events with the Cy5 located 11 bp 3' of the 1 nt Gap (5'-OH) was greater than the FRET efficiency of the TCC and STC events with the Cy5 located 11 bp 5' of the 1 nt Gap (5'-OH). These results are consistent with the conclusion that the Cy3-PFV intasome binds asymmetrically to the lesion-containing target DNA, with a preferred binding on the 3'-side of the 1 nt Gap (5'-OH). Nevertheless, the frequency of STC events appeared similar to the normalized counts of TCC FRET events (compare **Fig. 1e-g**, E > 0.1 with **Fig. 3a**, smFRET; **Extended Table 5**). These results suggest that the fluorophore location has little or no effect on TCC or STC events. Taken together we conclude that transient TCC events contribute to increased STC products.

Nicks and gaps direct site-specific PFV integration. To map the STC events we examined strand transfer products by denaturing gel electrophoresis (DGE; **Fig. 1a**, Gel; **Fig. 3b,c**). These studies incubated unlabeled PFV intasomes with the target DNAs utilized in the smFRET analysis (**Fig. 1a,b**; **Extended Data Table 1**). No integration events were observed in control reactions (-PFV) or with fully duplex target DNA (G/C) as well as target DNA containing an 8-Oxo-G (8-Oxo-G), G/T mismatch (G/T) or a +T insertion (+T). However, additional DNA bands of varying intensity were observed with a target DNA containing a Nick (5'-P or 5'-OH), a 1 nt Gap (5'-P or 5'-OH) or a 2 nt Gap (5'-P or 5'-OH) that are consistent with covalent PFV integration products (**Fig. 3b**). The pattern and frequency of STC events observed by smTIRF generally mimicked the Gel analysis (**Fig. 3a**), with differences in the absolute frequency of integration attributable to the lower concentration of PFV intasomes utilized in smFRET to moderate background fluorescence (5 nM smTIRF compared to 25 nM for Gel analysis).

Most strand transfer events observed by DGE were the result of half-site integration (**Fig. 3b**). For example, the target DNA containing a 1 nt Gap, Nick and 2 nt Gap with a 5'-P resulted in major Cy5-DNA bands of 82, 81, and 80 nt, respectively (**Fig. 3b**, left; see Key above). These correspond to covalent strand transfer of the 38 bp vDNA into the non-lesion containing Cy5-labeled strand 44, 43, 42 nt from the 3'-end, respectively (**Fig. 3c**). Since PFV integration events are separated by 4 bp [21,29], this strand transfer event would place the concerted strand transfer location on the lesion-containing strand at the 5'-side of the missing nucleotide within the 1 nt Gap, at the Nick or at the 5'-side of the second missing nucleotide of the 2 nt Gap. In all these cases there is no phosphate bond to complete the isoenergetic strand transfer chemistry. A similar integration pattern was detected with target DNAs containing a 1 nt Gap, Nick and 2 nt Gap with a 5'-OH (**Fig. 3b**, right). Importantly, the asymmetric location of these integration products corresponds with the asymmetric binding predicted by TCC and STC FRET events.

There were curious differences in band intensity and/or number when the 5'-P and 5'-OH lesions were compared (**Fig. 3b**). These include a substantial increase in the 82 nt product with

the target DNA containing a 1 nt Gap (5'-OH) and an apparent splitting of intensity between 82 nt and 80 nt products with the target DNA containing a 2 nt Gap (5'-OH) (**Fig. 3b**, right). The 80 nt and 82 nt products with the 2 nt Gap (5'-OH) is consistent with ~50% of the PFV intasomes positioning next to the 3'-OH and ~50% positioning next to the 5'-side of the second missing nucleotide similar to the 2 nt Gap (5'-P) (**Fig. 3c**). These results appear internally consistent with the broadening and shift to increased FRET efficiency of STC events observed by smFRET with target DNA containing a 2 nt Gap (5'-OH), and suggest that the presence of a 5'-P can influence the location of half-site strand transfer events by altering the stable positioning of PFV intasomes.

In addition, a 42 nt and 41 nt DNA product was also detected with the 1 nt Gap (5'-OH) and 2 nt Gap (5'-OH), respectively (**Fig. 3b**, right; **Fig. 3c**). These DNA products appear consistent with aborted strand transfer events that leave a strand scission on the non-lesion containing Cy5-labeled strand. In both cases, we would be unable to detect a corresponding strand transfer on the fluorophore-deficient lesion-containing strand. Moreover, a weak but clearly visible DNA product of ~76 nt with the target DNAs containing a 2 nt Gap (5'-OH) (**Fig. 3b**). This product could conceivable signify a concerted integration event since the second strand transfer should occur 35 nt from the 5'-end on the lesion-containing strand, which would also be undetectable with unlabeled PFV intasomes.

To determine whether additional integration events occur on the target DNA, we assembled PFV intasomes containing Cy3-labeled vDNA on the transferred strand (Cy3-PFV (TS); **Extended Data Table 1**). Cy3-PFV (TS) integration events transfer a 30 nt vDNA to an unlabeled target DNA (unlabeled), a target DNA containing a Cy5-fluorophore located 5' of the lesion on the non-lesion containing strand (F-Cy5) or a target DNA containing a Cy5-fluorophore located 3' on the lesion-containing strand (R-Cy5) (**Extended Data Table 1**). We examined the 1 nt Gap (5'-OH) and 2 nt Gap (5'-OH) target DNA substrates since they initially revealed integration products other than the major half-site strand transfer events (**Fig. 3b**). The principal Cy3-PFV (TS) integration events (>90%) produced fragments of 76 nt or 74 nt for both the 1 nt

Gap (5'-OH) and 2 nt Gap (5'-OH) (**Fig. 3d**; **Extended Data Fig. 11a**). Subtracting the 30 nt vDNA from the strand transfer product and accounting for a 2 nt apparent size increase when both a Cy3 and Cy5 fluorophore are present when compared to Cy3-labeled molecular weight markers, the calculated integration events occurred at 44 nt on the non-lesion containing strand (**Fig. 3d**; **Extended Data Fig. 11a,b**; black arrowhead). This is the identical location that produced the 80 nt and 82 nt half-site integration products with the unlabeled PFV intasomes (**Fig. 3b**). We also detected background levels of the 41 nt and 42 nt aborted strand transfer product with the F-Cy5 target DNA substrates (**Fig. 3d**; **Extended Data Fig. 11a,b**; red arrowhead) that would be undetectable with the R-Cy5 and Unlabeled Target DNAs (**Fig. 3d**; **Extended Data Fig. 11**; orange arrowhead).

Minor Cy3-PFV (TS) integration products were identified with 1 nt Gap (5'-OH) and 2 nt Gap (5'-OH) target DNA substrates (**Fig. 1d**, black dots), that could be enhanced by increasing the image contrast (**Extended Data Fig. 11a,b**). These additional integration events accounted for < 5% of the target DNA integration products, with the majority localized around the lesion (gray arrows) and including a distinct concerted integration product adjacent to the lesion (red dashed arrow; **Fig. 1d**, bottom). We note that half-site integration products mapped to 26 nt and 28 nt on the F-Cy5 target DNA could also be localized to the non-lesion containing strand at 11 nt and 13 nt, respectively, and are therefore marked with a star (**Fig. 1d**, bottom). The 26, 28, 45 and 48 integration products appeared to be equidistant pairs from with the Cy5 fluorophore location (**Fig. 1d**), suggesting other DNA lesions might also enhance retroviral integration. More products could be visualized with increased image contrast but accounted for an even more minor fraction of the events. Together, these results confirm the conclusion that target DNA mimicking BER intermediates significantly enhances integration at the site of the lesion.

Target DNA Binding and Integration does not substantially alter the PFV intasome structure. Whether TCC and STC events provoke a conformational transition within the PFV

intasome is unknown. To address this question, we designed a smFRET system in which alterations in the relative geometry of the vDNA could be monitored with high precision (**Fig. 4a**). PFV intasomes were assembled with two donor vDNAs, one containing a Cy3 fluorophore and the other containing a Cy5 fluorophore (Cy3/Cy5-PFV; **Fig. 4a,b**; **Online Methods**). Structural studies suggest that the position of the vDNA within the TCC and STC are nearly identical with similarly identical calculated FRET efficiency (**Fig. 4b**) [21,29]. These structures have retained IN subunits that appear to localize the vDNA [21,29]. The stability and dynamics of these IN subunits during TCC and STC formation has not been determined [21,29].

The relative vDNA geometry in the Cy3/Cy5-PFV was examined during interactions with the model 1 nt Gap (5'-OH) target DNA that displayed the greatest TCC and STC formation. We first localized the 1 nt Gap (5'-OH) target DNA in the smFRET flow cell and then photobleached the identifying Cy5 fluorophore prior to injection of Cy3/Cy5-PFV intasomes. Transient TCC events similar to those observed with the Cy3-PFV intasomes were frequent and displayed a broad FRET peak with trailing less frequent lower FRET events (100 msec frame rate; $E_{Cy3/Cy5\text{-}PFV}$ = 0.62 ± 0.1, mean ± 1σ; **Fig. 4c**; **Extended Data Fig. 12**). These observations suggest that formation of a TCC on 1 nt Gap (5'-OH) target DNA generally broadened the distance between the vDNAs compared to the distance calculated from the structural studies. Moreover, the broad FRET distribution appears consistent with significant TCC structural dynamics.

In contrast, the formation of a stable STC by Cy3/Cy5-PFV intasomes on the 1 nt Gap (5'-OH) target DNA resulted in a narrower distribution of higher FRET events with fewer trailing lower FRET events (1 sec frame rate; $E_{Cy3/Cy5\text{-}PFV}$ = 0.69 ± 0.06, mean ± 1σ; **Fig. 4d**). A similar narrower distribution with significantly fewer STC events was detected at 100 msec frame rate ($E_{Cy3/Cy5\text{-}PFV}$ = 0.66 ± 0.09, mean ± 1σ; **Extended Data Fig. 12**). Both the TCC and STC events displayed a lower FRET efficiency than calculated from the crystal structures. This observation suggests that the intasome complexes are likely to enjoy a more open configuration in solution. We noted a

peak of very low pseudo-FRET events that appeared when the studies were performed at 1 sec frame rate (6% of the products). When examined individually these pseudo-FRET events were found to result from STC events by Cy3/Cy3-PFV intasomes containing two Cy3-vDNAs. Excitation of these Cy3/Cy3-PFV STC events resulted in bleed-through to the Cy5 channel. When we added these to the total number of STC events (see *) as well as the calculated frequency of Cy5/Cy5-PFV intasome STC events that are undetectable with this smFRET system (~5%), the total frequency of STC events with these Cy3+Cy5 vDNA PFV intasomes (~21%) is near equivalent to the frequency of STC events observed with the Cy3-PFV intasomes (20%). Overall these results suggest that the STC events result in a relatively stable vDNA geometry on the target DNA. Since four-way DNA is dynamic even in the absence of nicks or gaps at the junction that should further increase mobility [45], these observations suggest that following STC formation a stable integrase complex remains associated with the covalent vDNA-target DNA structure.

DISCUSSION

Previous single molecule analysis of PFV intasome has demonstrated that the identification of a suitable DNA site limits integration [22]. Once located the concerted strand transfer steps appear to occur in < 0.5 sec [22]. Biochemical and structural studies have suggested that retroviruses prefer bent and/or flexible DNA at the integration site [19,21,23,43]. Here we show that intrinsically flexible but intact duplex DNA containing a G/T mismatch or a +T nucleotide insertion that stably induces a DNA bend does not significantly enhance binding or integration of PFV intasomes. Because the substrates and structures previously examined also alter the twist of the duplex target, we consider the possibility that it is the recognition of a stable or transiently untwisted DNA that may constitute the actual preferred PFV intasome integration site. This conclusion is consistent with the PFV intasome preference for supercoiled DNA [22], which undergoes continuous and dynamic exchange between plectonemic coils and untwisted duplex DNA [46].

A preference for bent DNA with many degrees-of-freedom not generally observed with intact duplex DNA is consistent with the enhanced binding and integration into nicked and gapped target DNAs observed here. We also observed asymmetric binding and integration into the nicked and gapped target DNA that appears to place the intasome on the 3'side of the lesion. It is interesting to note that this asymmetry places the first nucleotide 5' of the two strand transfer sites within a gap lesion. It seems possible that the 5'-G preference in HIV integration sites reflects targeting to sites where OGG1 has created a gap following removal of an 8-oxo-G lesion. However, in the absence of a phosphate bond within the gap these targeted events may largely be half-site integration products that should result in a double strand break (DSB). In order to obtain a concerted integration, the gap must be repaired before the intasome is disassembled or a DSB is formed. Interestingly, MUTYH has been found to interact with abasic (AP) sites shielding them from the AP endonuclease (APE) that creates a nick at the AP site, thus preserving the phosphate bond [47]. MUTYH also interacts with the RAD9-RAD1-HUS1 (9-1-1) DSB signaling complex [48]. Perhaps a combination of OGG1 and MUTYH activities may both create a DNA lesion that would target retrovirus binding as well as the components necessary to recover some concerted integration products from the largely half-site integration events. In this scenario, the loss of 5'-G preference in the consensus HIV integration sites from *OGG1* mutant cells is due to the loss of integration products where the HIV genome has been eliminated by DSB repair. All of these models assume that PFV and HIV intasomes are targeted similarly by nicked or gapped target DNA.

The Cy3/Cy5-PFV smFRET studies strongly suggest that the intasome complex remains associated with the target DNA following an integration event (**Fig. 4**). Single molecule magnetic tweezer studies have suggested that under very low force (~0.1 pN), any bound integration complex allows free-rotation of DNA strands that released supercoils as well as dissociation of a DSB induced by an integration event [Jones, 2016 #15561]. Subsequent studies have suggested that the intasome complex may be stable enough to tether the DSB ends even at high force (>30

pN) [Vanderlinden, 2019 #16568]. However, these latter studies appear to have left the reaction on ice for extended periods of time prior to force induction. Under these conditions PFV intasome undergo significant aggregation and inactivation (Rabe et al., submitted). It seems plausible that the high force stability largely reflects half-site integration products that would be tethered by the unintegrated single stranded DNA. Nevertheless, our smFRET studies suggest that the IN subunits stabilize the vDNA geometry following integration albeit in a slightly more open configuration than predicted by the crystal structure.

Adaptation of genomic integration properties has been employed in the development of gene delivery vehicles designed to correct a variety of monogenic diseases [49]. Lentiviral vectors derived from the HIV-1 retrovirus are most easily manipulated and can infect non-dividing cells [50]. However, HIV-1 often integrates into open actively transcribing host genomic regions [51], which may unintentionally alter cellular functions or activate oncogenes [52]. Modulating non-pathogenic retrovirus target site choice is one scheme for altering genome targeting. The results presented here suggest that modifying the DNA configuration of a target site may be an additional method for targeted gene therapy.

METHODS

Methods are included in a separate document for online publication.

Acknowledgments

The authors would like to thank Ryan Messer and Yow-Yong Tan for technical assistance, Rob Levendosky, and Gregory Bowman (John Hopkins University) for providing protocols for the sequencing ladder. This work was supported by the National Institutes of Health (AI126742 to R.F. & K.E.Y and GM121284 to K.E.Y).

Author contributions

R.F., K.Y. and G.S. conceived, designed, and analyzed the smFRET experiments. A.G. performed and analyzed the integration site mapping experiments. J.L. wrote the MATLAB code for smFRET data analysis. R.F., K.Y., G.S., A.G., and R.K.M wrote the manuscript.

Competing financial interests

The authors declare no competing financial interests.

Additional information

Any supplementary information and source data are available in the online version of the paper. Correspondence and requests for materials should be addressed to K.Y. or R.F.

FIGURE LEGENDS

Figure 1. Visualizing the dynamics of PFV INT TC in real-time. (**a**) The smFRET experimental setup for visualizing TC by a PFV INT labeled with 2Cy3s on non-transfer strands at a proximal position (NTS-P) to the core. The INT was introduced onto various tDNAs containing A488 and Cy5 (**b**) A representative intensity trajectory (panel 1), the corresponding FRET trajectory with the HMM fitting (panel 2), the TDP with arrows pointing to the major peaks (panel 3) and the PSH (panel 4) displaying INT aggregation events for 8-Oxo G DNA. (**c**) A representative intensity trajectory (panel 1), the corresponding FRET trajectory with the HMM fitting (panel 2), the TDP with arrows pointing to the major peaks (panel 3) and the PSH (panel 4) displaying transient events for 5'-P 1nt Gap DNA. (**d**) The TDP with arrows pointing to the major peaks (panel 1) and the PSH (panel 2) displaying transient events for 5'-P Nick DNA. (**e**) The TDP with arrows pointing to the major peaks (panel 1) and the PSH (panel 2) displaying transient events for 5'-P 2nt Gap DNA. (**f**) smFRET histograms showing the distribution of E_{aggn} and E_{TCC} for the above tDNAs (panel 1). The TCC (panel 2) and the dissociated state (panel 3) lifetimes of INT for tDNAs that showed E_{TCC}. Error bars in dwell times represent errors from the fittings of dwell time distributions shown in **Supplementary Fig. 7**. *N* is the number of DNA molecules included in each analysis. The color scales indicate the normalized frequencies of FRET transitions included in TDPs and PSHs.

Figure 2. Testing different tDNAs for dynamic TC in real-time

(**a-e**) The TDP with arrows pointing to the major peaks (panel 1) and the PSH (panel 2) displaying transient events for GT MM DNA (**a**), T-Bulge DNA (**b**), 5'-OH 1nt Gap DNA (**c**), 5'-OH Nick DNA (**d**) and 5'-OH 2nt Gap DNA (**e**). (**f**) smFRET histograms displaying the distribution of E_{aggn} and E_{TCC} for the above tDNAs (panel 1). The TCC lifetimes of INT for DNA substrates that showed E_{TCC} (panel 2). (**g**) The dissociated state lifetime of INTs for DNA substrates that showed $E_{TCC.}$ Error bars in dwell times represent errors from the fittings of dwell time distributions shown in

Supplementary Fig. 7. These data were collected using an smFRET setup similar to **Fig. 1a**. *N* is the number of DNA molecules included in each analysis. The color scales indicate the normalized frequencies of FRET transitions included in TDPs and PSHs.

Figure 3. Visualizing the PFV INT catalyzed ST in real-time

(**a-c**) Representative intensity trajectories and corresponding FRET trajectories with HMM fittings showing ST by the NTS-P-2Cy3-PFV INTwt construct. The photobleaching of Cy3 and Cy5 are denoted by green and red arrows respectively. (**d,e**) The PSH and the smFRET histogram for 5'-P 1nt Gap DNA (**d**) and 5'-OH 1nt Gap DNA (**e**) displaying STC events. The Gaussian fits to the smFRET histograms are shown as red lines. These data were collected at 1 s resolution using a smFRET setup similar to **Fig. 1a**. The number of DNA molecules (*N*) that showed STC formation and corresponding %STCs are shown. The color scale indicates the normalized frequencies of FRET transitions included in PSHs. (**f**) %STC obtained in the SM assays for different tDNAs with the NTS-P-2Cy3-PFV INTwt construct alongside quantification of the bulk activity assay. The error bars in the SM data reflect $\frac{\sqrt{N}}{N_{Total}} \times 100\%$. The error bars in the bulk activity data reflect standard deviation from triplicates. (**g**) A scheme showing the analysis of integration sites for 5'-OH 1 nt Gap DNA (top) and denaturing PAGE gels showing the products from the bulk integration assays (bottom). The lengths of ssDNA and fluorophore locations are shown. The nicked and 2 nt substrates respectively contained 40 nt and 38 nt ssDNA in the place of 39 nt strand (**Supplementary Tables 1,2**). All the other substrates contained continues ssDNA with the corresponding lesion, 5'-Biotin and A488 closer to the 3'-end as the top strand (**Supplementary Table 1,2**).

Figure 4. Probing structural dynamics of the PFV INT during TC and ST. (**a**) The smFRET experimental setup for visualizing structural dynamics of PFV INT during TCC and STC formation.

A PFV INT labeled with Cy3 and Cy5 at the non-transfer strands (NTS-Cy3-Cy5-PFVwt INT) was introduced onto various tDNAs after photobleaching Cy5 attached to the tDNAs. (**b**) A representative intensity trajectory and corresponding FRET trajectory with the HMM fitting (panel 1), the TDP with arrows pointing to the major peaks (panel 2), the PSH and the smFRET histogram (panel 3) displaying transient TC on 5'-OH 1nt Gap DNA at 100 ms resolution. (**c**) Representative intensity, FRET and HMM traces acquired at 1 s resolution with the NTS-Cy3-Cy5-PFVwt INT and 5'-OH 1nt Gap DNA showing the real time formation of STCs (panel 1,2). The resultant PSH and the smFRET histogram for STC traces (panel 3). The photo blinking and photobleaching of Cy5 are denoted by red arrows. The blue arrows indicate random floating aggregates of INTs that occasionally produced pseudo FRET transitions. The Gaussian fits to smFRET histograms are shown as red lines. *N* is the number of DNA molecules included in each analysis. The %STC is also shown in the PSH of STCs. The color scales indicate the normalized frequencies of FRET transitions included in the TDP and the PSH.

Figure 5. Kinetics and dynamics of asymmetric TC leading asymmetric STCs. (a) PFV INT in solution may bind to a tDNA and reach a lesion using the rotational coupled 1D diffusion. Tracking of the tDNA backbone this way may allow the INT to engage with the damage site efficiently. Association of one vDNA end with the 5' side of a SSDB leads to asymmetric kinetic trapping of INT. During the short TCC lifetime, the other vDNA end can undergo ST to produce half-site integrations. The exceptional stability of this STC may require an active removal of IN, leading to the dissociation of unreactive vDNA as well. An symmetric TCC model, which was not observed, predicts STs on either side of the damage leading to concerted integrations. (**b**) Gibbs free energy landscape derived from the kinetic data for the 5'-OH 1nt Gap DNA and transition state theory. The free energy surface for the INs removal step was hypothetical and based on the exceptional stability of STCs.

References

1. Varmus, H. Retroviruses. *Science* **240**, 1427-35 (1988).
2. Bowerman, B., Brown, P.O., Bishop, J.M. & Varmus, H.E. A nucleoprotein complex mediates the integration of retroviral DNA. *Genes Dev* **3**, 469-78 (1989).
3. Wei, S.Q., Mizuuchi, K. & Craigie, R. A large nucleoprotein assembly at the ends of the viral DNA mediates retroviral DNA integration. *EMBO J* **16**, 7511-20 (1997).
4. Lesbats, P., Engelman, A.N. & Cherepanov, P. Retroviral DNA Integration. *Chem Rev* **116**, 12730-12757 (2016).
5. Delelis, O., Carayon, K., Saib, A., Deprez, E. & Mouscadet, J.F. Integrase and integration: biochemical activities of HIV-1 integrase. *Retrovirology* **5**, 114 (2008).
6. Brown, P.O., Bowerman, B., Varmus, H.E. & Bishop, J.M. Retroviral integration: structure of the initial covalent product and its precursor, and a role for the viral IN protein. *Proc Natl Acad Sci U S A* **86**, 2525-9 (1989).
7. Roth, M.J., Schwartzberg, P.L. & Goff, S.P. Structure of the termini of DNA intermediates in the integration of retroviral DNA: dependence on IN function and terminal DNA sequence. *Cell* **58**, 47-54 (1989).
8. Espeseth, A.S. et al. siRNA screening of a targeted library of DNA repair factors in HIV infection reveals a role for base excision repair in HIV integration. *PLoS One* **6**, e17612 (2011).
9. Yoder, K.E. et al. The base excision repair pathway is required for efficient lentivirus integration. *PLoS One* **6**, e17862 (2011).
10. Yoder, K.E. & Bushman, F.D. Repair of gaps in retroviral DNA integration intermediates. *J Virol* **74**, 11191-200 (2000).
11. Holman, A.G. & Coffin, J.M. Symmetrical base preferences surrounding HIV-1, avian sarcoma/leukosis virus, and murine leukemia virus integration sites. *Proc Natl Acad Sci U S A* **102**, 6103-7 (2005).
12. Wu, X., Li, Y., Crise, B., Burgess, S.M. & Munroe, D.J. Weak palindromic consensus sequences are a common feature found at the integration target sites of many retroviruses. *J Virol* **79**, 5211-4 (2005).
13. Barnes, D.E. & Lindahl, T. Repair and genetic consequences of endogenous DNA base damage in mammalian cells. *Annu Rev Genet* **38**, 445-76 (2004).
14. Ciccia, A. & Elledge, S.J. The DNA damage response: making it safe to play with knives. *Mol Cell* **40**, 179-204 (2011).
15. Bennett, G.R. et al. Repair of oxidative DNA base damage in the host genome influences the HIV integration site sequence preference. *PLoS One* **9**, e103164 (2014).
16. Hegde, M.L., Hazra, T.K. & Mitra, S. Early steps in the DNA base excision/single-strand interruption repair pathway in mammalian cells. *Cell Res* **18**, 27-47 (2008).
17. Robertson, A.B., Klungland, A., Rognes, T. & Leiros, I. DNA repair in mammalian cells: Base excision repair: the long and short of it. *Cell Mol Life Sci* **66**, 981-93 (2009).
18. Friedberg, E.C. A history of the DNA repair and mutagenesis field: The discovery of base excision repair. *DNA Repair (Amst)* **37**, A35-9 (2016).
19. Pruss, D., Reeves, R., Bushman, F.D. & Wolffe, A.P. The influence of DNA and nucleosome structure on integration events directed by HIV integrase. *J Biol Chem* **269**, 25031-41 (1994).
20. Bor, Y.C., Bushman, F.D. & Orgel, L.E. In vitro integration of human immunodeficiency virus type 1 cDNA into targets containing protein-induced bends. *Proc Natl Acad Sci U S A* **92**, 10334-8 (1995).
21. Maertens, G.N., Hare, S. & Cherepanov, P. The mechanism of retroviral integration from X-ray structures of its key intermediates. *Nature* **468**, 326-9 (2010).

22. Jones, N.D. et al. Retroviral intasomes search for a target DNA by 1D diffusion which rarely results in integration. *Nat Commun* **7**, 11409 (2016).
23. Maskell, D.P. et al. Structural basis for retroviral integration into nucleosomes. *Nature* **523**, 366-9 (2015).
24. Fuller, J.R. & Rice, P.A. Target DNA bending by the Mu transpososome promotes careful transposition and prevents its reversal. *Elife* **6**(2017).
25. Jones, N.D. et al. Prototype foamy virus intasome aggregation is mediated by outer protein domains and prevented by protocatechuic acid. *Sci Rep* **9**, 132 (2019).
26. Wilson, M.D. et al. Retroviral integration into nucleosomes through DNA looping and sliding along the histone octamer. *Nat Commun* **10**, 4189 (2019).
27. Yin, Z. et al. Crystal structure of the Rous sarcoma virus intasome. *Nature* **530**, 362-6 (2016).
28. Vanderlinden, W. et al. The free energy landscape of retroviral integration. *Nat Commun* **10**, 4738 (2019).
29. Hare, S., Gupta, S.S., Valkov, E., Engelman, A. & Cherepanov, P. Retroviral intasome assembly and inhibition of DNA strand transfer. *Nature* **464**, 232-6 (2010).
30. Cook, N.J. et al. Structural basis of second-generation HIV integrase inhibitor action and viral resistance. *Science* **367**, 806-810 (2020).
31. Passos, D.O. et al. Structural basis for strand-transfer inhibitor binding to HIV intasomes. *Science* **367**, 810-814 (2020).
32. Roy, R., Hohng, S. & Ha, T. A practical guide to single-molecule FRET. *Nat Methods* **5**, 507-16 (2008).
33. Mills, J.B., Cooper, J.P. & Hagerman, P.J. Electrophoretic evidence that single-stranded regions of one or more nucleotides dramatically increase the flexibility of DNA. *Biochemistry* **33**, 1797-803 (1994).
34. Guo, H. & Tullius, T.D. Gapped DNA is anisotropically bent. *Proc Natl Acad Sci U S A* **100**, 3743-7 (2003).
35. Roll, C., Ketterle, C., Faibis, V., Fazakerley, G.V. & Boulard, Y. Conformations of nicked and gapped DNA structures by NMR and molecular dynamic simulations in water. *Biochemistry* **37**, 4059-70 (1998).
36. Zhang, Y. & Crothers, D.M. High-throughput approach for detection of DNA bending and flexibility based on cyclization. *Proc Natl Acad Sci U S A* **100**, 3161-6 (2003).
37. Bronson, J.E., Fei, J., Hofman, J.M., Gonzalez, R.L., Jr. & Wiggins, C.H. Learning rates and states from biophysical time series: a Bayesian approach to model selection and single-molecule FRET data. *Biophys J* **97**, 3196-205 (2009).
38. Senavirathne, G., Mahto, S.K., Hanne, J., O'Brian, D. & Fishel, R. Dynamic unwrapping of nucleosomes by HsRAD51 that includes sliding and rotational motion of histone octamers. *Nucleic Acids Res* **45**, 685-698 (2017).
39. Isaacs, R.J., Rayens, W.S. & Spielmann, H.P. Structural differences in the NOE-derived structure of G-T mismatched DNA relative to normal DNA are correlated with differences in (13)C relaxation-based internal dynamics. *J Mol Biol* **319**, 191-207 (2002).
40. Isaacs, R.J. & Spielmann, H.P. A model for initial DNA lesion recognition by NER and MMR based on local conformational flexibility. *DNA Repair (Amst)* **3**, 455-64 (2004).
41. Joshua-Tor, L. et al. Three-dimensional structures of bulge-containing DNA fragments. *J Mol Biol* **225**, 397-431 (1992).
42. Muller, H.P. & Varmus, H.E. DNA bending creates favored sites for retroviral integration: an explanation for preferred insertion sites in nucleosomes. *EMBO J* **13**, 4704-14 (1994).
43. Pruss, D., Bushman, F.D. & Wolffe, A.P. Human immunodeficiency virus integrase directs integration to sites of severe DNA distortion within the nucleosome core. *Proc Natl Acad Sci U S A* **91**, 5913-7 (1994).

44. Jeong, C. et al. MutS switches between two fundamentally distinct clamps during mismatch repair. *Nat Struct Mol Biol* **18**, 379-85 (2011).
45. McKinney, S.A., Freeman, A.D., Lilley, D.M. & Ha, T. Observing spontaneous branch migration of Holliday junctions one step at a time. *Proc Natl Acad Sci U S A* **102**, 5715-20 (2005).
46. van Loenhout, M.T.J., de Grunt, M.V. & Dekker, C. Dynamics of DNA Supercoils. *Science* **338**, 94-97 (2012).
47. Raetz, A.G. et al. The DNA repair enzyme MUTYH potentiates cytotoxicity of the alkylating agent MNNG by interacting with abasic sites. *J Biol Chem* **295**, 3692-3707 (2020).
48. Luncsford, P.J. et al. A structural hinge in eukaryotic MutY homologues mediates catalytic activity and Rad9-Rad1-Hus1 checkpoint complex interactions. *J Mol Biol* **403**, 351-70 (2010).
49. Yoder, K.E., Rabe, A.J., Fishel, R. & Larue, R.C. Strategies for Targeting Retroviral Integration for Safer Gene Therapy: Advances and Challenges. *Front Mol Biosci* **8**, 662331 (2021).
50. Poeschla, E., Corbeau, P. & Wong-Staal, F. Development of HIV vectors for anti-HIV gene therapy. *Proc Natl Acad Sci U S A* **93**, 11395-9 (1996).
51. Schroder, A.R. et al. HIV-1 integration in the human genome favors active genes and local hotspots. *Cell* **110**, 521-9 (2002).
52. Kohn, D.B., Sadelain, M. & Glorioso, J.C. Occurrence of leukaemia following gene therapy of X-linked SCID. *Nat Rev Cancer* **3**, 477-88 (2003).

Fig. 1

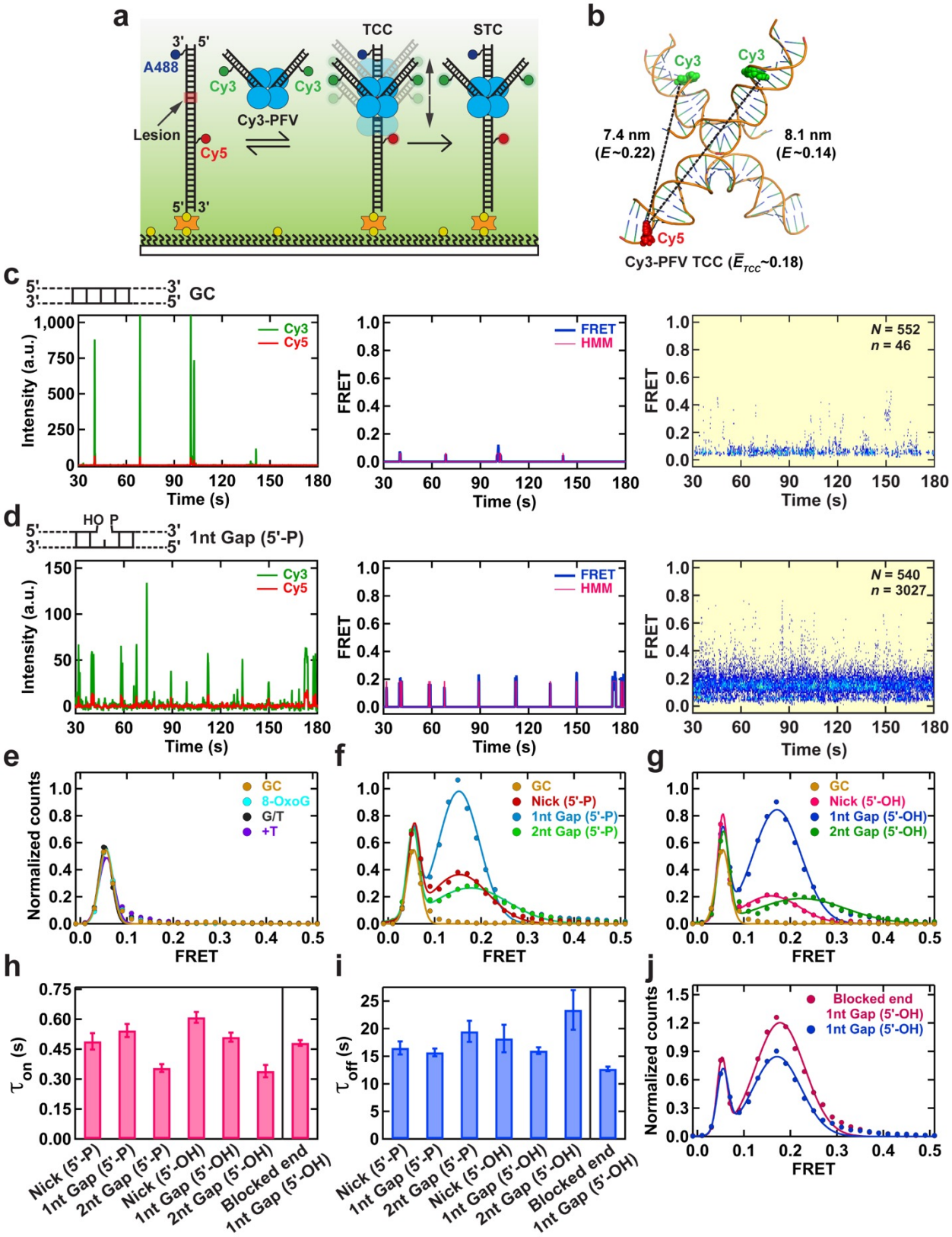
a
3'
5'
A488
Lesion
Cy5
5'
3'
Cy3
Cy3
Cy3-PFV
TCC
STC
b
Cy3
Cy3
7.4 nm
(E~0.22)
8.1 nm
(E~0.14)
Cy5
Cy3-PFV TCC (Ē_TCC~0.18)
c
5'
3'
3'
5'
GC
Intensity (a.u.)
Cy3
Cy5
Time (s)
FRET
HMM
N = 552
n = 46
d
HO P
1nt Gap (5'-P)
N = 540
n = 3027
e
Normalized counts
GC
8-OxoG
G/T
+T
FRET
f
GC
Nick (5'-P)
1nt Gap (5'-P)
2nt Gap (5'-P)
g
GC
Nick (5'-OH)
1nt Gap (5'-OH)
2nt Gap (5'-OH)
h
τon (s)
Nick (5'-P)
1nt Gap (5'-P)
2nt Gap (5'-P)
Nick (5'-OH)
1nt Gap (5'-OH)
2nt Gap (5'-OH)
Blocked end
1nt Gap (5'-OH)
i
τoff (s)
j
Blocked end
1nt Gap (5'-OH)
1nt Gap (5'-OH)

Fig. 2

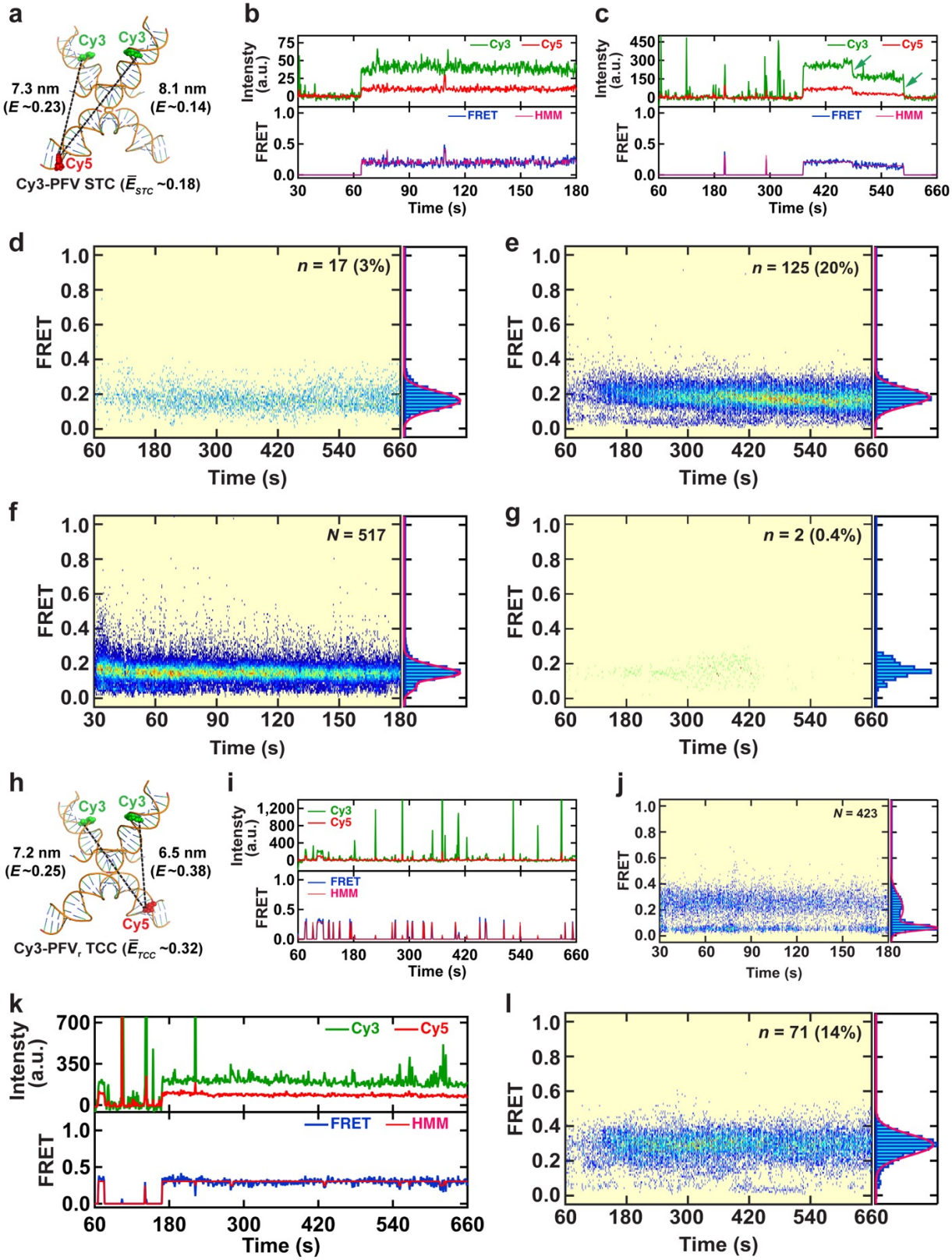
a
Cy3
Cy3
7.3 nm
(E ~0.23)
8.1 nm
(E~0.14)
Cy5
Cy3-PFV STC ($\bar{E}_{STC}$ ~0.18)
b
Intensity (a.u.)
Cy3
Cy5
FRET
HMM
Time (s)
c
Intensity (a.u.)
Cy3
Cy5
FRET
HMM
Time (s)
d
n = 17 (3%)
FRET
Time (s)
e
n = 125 (20%)
FRET
Time (s)
f
N = 517
FRET
Time (s)
g
n = 2 (0.4%)
FRET
Time (s)
h
Cy3
Cy3
7.2 nm
(E~0.25)
6.5 nm
(E~0.38)
Cy5
Cy3-PFV$_r$ TCC ($\bar{E}_{TCC}$ ~0.32)
i
Intensity (a.u.)
Cy3
Cy5
FRET
HMM
Time (s)
j
N = 423
FRET
Time (s)
k
Intensity (a.u.)
Cy3
Cy5
FRET
HMM
Time (s)
l
n = 71 (14%)
FRET
Time (s)

Fig. 3

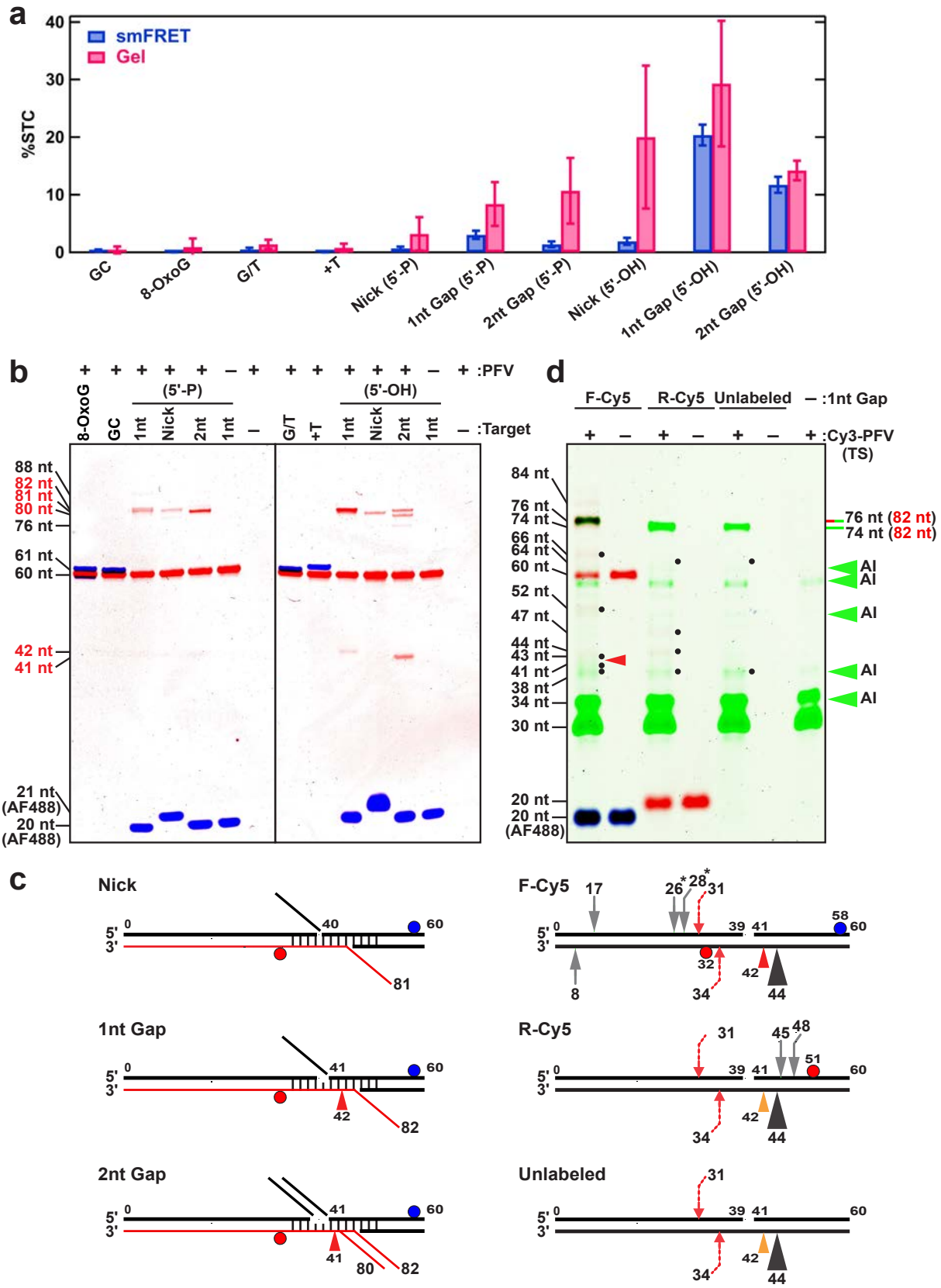
a
smFRET
Gel
%STC
40
30
20
10
0
GC
8-OxoG
G/T
+T
Nick (5'-P)
1nt Gap (5'-P)
2nt Gap (5'-P)
Nick (5'-OH)
1nt Gap (5'-OH)
2nt Gap (5'-OH)
b
:PFV
(5'-P)
(5'-OH)
:Target
88 nt
82 nt
81 nt
80 nt
76 nt
61 nt
60 nt
42 nt
41 nt
21 nt (AF488)
20 nt (AF488)
d
F-Cy5
R-Cy5
Unlabeled
:1nt Gap
:Cy3-PFV (TS)
84 nt
76 nt
74 nt
66 nt
64 nt
60 nt
52 nt
47 nt
44 nt
43 nt
41 nt
38 nt
34 nt
30 nt
20 nt
20 nt (AF488)
76 nt (82 nt)
74 nt (82 nt)
AI
c
Nick
1nt Gap
2nt Gap
F-Cy5
R-Cy5
Unlabeled
5'
3'

Fig. 4

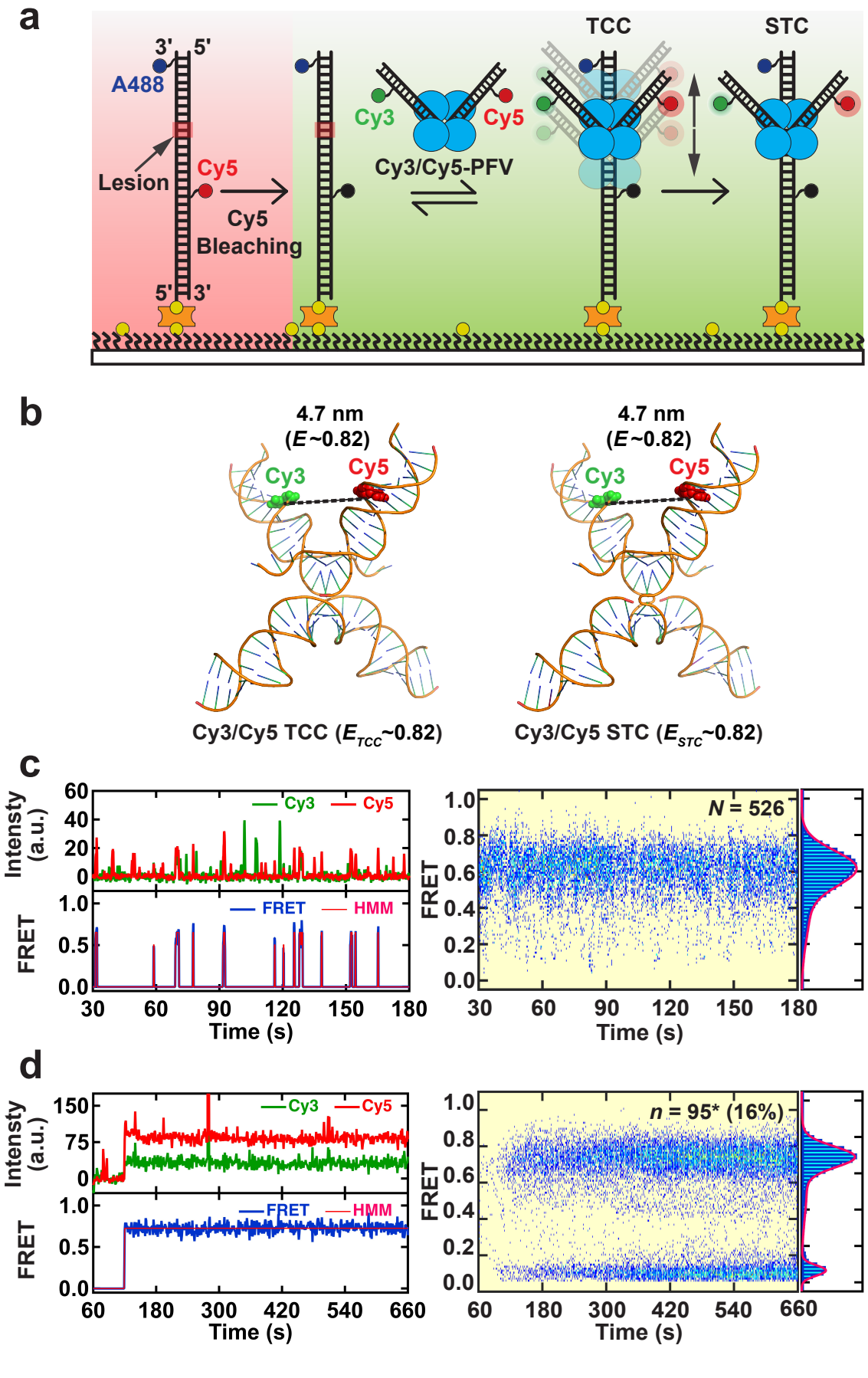
a
3'
5'
A488
Lesion
Cy5
Cy5
Bleaching
5'
3'
Cy3
Cy5
Cy3/Cy5-PFV
TCC
STC
b
4.7 nm
(E~0.82)
Cy3
Cy5
Cy3/Cy5 TCC (E_TCC~0.82)
4.7 nm
(E~0.82)
Cy3
Cy5
Cy3/Cy5 STC (E_STC~0.82)
c
Intensity (a.u.)
Cy3
Cy5
FRET
FRET
HMM
Time (s)
N = 526
FRET
Time (s)
d
Intensity (a.u.)
Cy3
Cy5
FRET
FRET
HMM
Time (s)
n = 95* (16%)
FRET
Time (s)